

Automated quantum operations in photonic qutritsG. F. Borges,^{1,*} R. D. Baldijão,^{1,2} J. G. L. Condé,¹ J. S. Cabral,³ B. Marques,⁴ M. Terra Cunha,⁵ A. Cabello,⁶ and S. Pádua¹¹*Departamento de Física, Universidade Federal de Minas Gerais, Belo Horizonte, MG 31270-901, Minas Gerais, Brazil*²*Instituto de Física Gleb Wataghin, Universidade Estadual de Campinas, Campinas, SP 13083-859, Brazil*³*Instituto de Física, Universidade Federal de Uberlândia, 38400-902, Uberlândia, MG, Brazil*⁴*Instituto de Física, Universidade de São Paulo, SP 05315-970, Brazil*⁵*Instituto de Matemática, Estatística e Computação Científica, 13083-859, Universidade de Campinas, Campinas, SP, Brazil*⁶*Departamento de Física Aplicada II, Universidad de Sevilla, E-41012 Sevilla, Spain*

(Received 13 November 2017; published 2 February 2018)

We report an experimental implementation of automated state transformations on spatial photonic qutrits following the theoretical proposal made by Baldijão *et al.* [*Phys. Rev. A* **96**, 032329 (2017)]. A qutrit state is simulated by using three Gaussian beams, and after some state operations, the transformed state is available in the end in terms of the basis state. The state transformation setup uses a spatial light modulator and a calcite-based interferometer. The results reveal the usefulness of the operation method. The experimental data show a good agreement with theoretical predictions, opening possibilities for explorations in higher dimensions and in a wide range of applications. This is a necessary step in qualifying spatial photonic qutrits as a competitive setup for experimental research in the implementation of quantum algorithms which demand a large number of steps.

DOI: [10.1103/PhysRevA.97.022301](https://doi.org/10.1103/PhysRevA.97.022301)**I. INTRODUCTION**

Quantum states of high dimensions (dimension $d > 2$) are important in many aspects of quantum theory, such as fundamental tests of quantum physics [1–5], quantum information and computation [6,7], and quantum key distribution [8,9]. Photonic qutrits prepared in terms of angular momentum states or photon transversal paths have been the subject of different quantum mechanical investigations. Other works have reconstructed qutrit density matrices via quantum tomography [10–14], quantified the amount of entanglement [15], realized entanglement witnesses and entanglement concentration in the laboratory [16–18], simulated quantum open system dynamics [19], produced cloning of qutrit states [20], and implemented noncontextuality tests [3,21,22].

A common technique in some of the previous works is the preparation of so-called *slit qutrits*: d slits placed in the transverse path of photons allow one to define a d -dimensional space state where quantum superpositions can be optically manipulated and tested. The main advantage of this approach is the possibility of high-dimensional state generation by increasing the number of slits [23–25]. If two multislit sets are placed in the path of two noncollinear photons generated by spontaneous parametric down-conversion (SPDC), a two-qubit photonic path state is prepared. A quantum state can be propagated immediately after the multislit planes by using a lens set, and spatial correlation at the multislit planes are also propagated to the image planes [26]. Typically, the characterization of slit qutrits is done in one of the following planes: image or Fourier. The first reads the modulus of the diagonal terms of the density operator in the slit basis, while the second serves

to test coherence. However, a central issue in working with a qutrit in slit states is that it is not a simple approach to apply a quantum operation and transform these states into a new superposition of the basis states. For this reason, projective measurements in different bases require operations at the Fourier plane which discard the encoding on the slit states [21,27]. This technique permits us to acquire the probability of the projection operation, but it does not deliver the projected qutrit in a superposition state in the basis states, imposing barriers to the application of such a technique. In recent years, the manipulation of those slit qutrits received the aid of spatial light modulators (SLMs), used to modulate both the phase and amplitude of each path mode [10,16,27,28], which allows automation of the processes, but did not bypass the problem of realizing nondiagonal operations. Here, we demonstrate the implementation of a recently proposed technique [29] in order to manipulate spatial qutrit states. After reviewing the central points of this technique, we show the realization of projections over some representative quantum states, as well as cyclic permutation operators on a qutrit. One central advantage is that the decision of which transformation to apply is communicated to the system by programming the SLM. This is an important step in the automatization of such a setup, allowing for flexibility and a certain degree of integrability in sequential quantum operations. The technique presented here tests important quantum state operations by using three Gaussian laser beams to simulate a qutrit state in a path variable instead of the usual slit states. This system is isomorphic with a qutrit Hilbert space, and since the operations are independent of the initial state, the results presented here are the same as expected for a single-photon qutrit encoded at transverse Gaussian paths. State transformations of qutrits encoded in the Gaussian spatial modes of the photon state usually require handmade interferometers [3,30]. Here, an

*gfbj@fisica.ufmg.br

interferometer is used only to sum up all the paths erasing which path information, while diffraction gratings displayed at the programmable SLM screen are responsible for defining the operation being implemented. A review of these steps follows below.

II. AUTOMATED OPERATIONS IN SINGLE-PHOTON MULTIPATH QUTRIT

Let us consider a single-photon source in which three parallel transverse Gaussian paths can be generated. This system is represented in the preparation frame of Fig. 1. Here, an attenuated Gaussian laser beam, having one photon per mode and propagating in the \hat{z} direction, passes through the calcite beam displacers (that separate the horizontal and vertical polarization components by 3 mm), half- and quarter-wave plates, and a polarizing beam splitter (PBS). The photon path state is given by

$$|\Psi\rangle = \sum_{\nu=0}^2 A_{\nu} |v\rangle_x \otimes |0\rangle_y \otimes |H\rangle, \quad (1)$$

where $|H\rangle$ represents the horizontal polarization state, while $|0\rangle_y$ represents a Gaussian path state in the \hat{y} direction centered in $y = 0$, A_{ν} are the amplitudes associated with the path state components ν and $|v\rangle_x = \int_{-\infty}^{\infty} dx \exp\{-\frac{[x-\nu d]^2}{2\sigma^2}\} |1x\rangle$, where $|1x\rangle$ is the Fourier transform of the Fock state $|1q\rangle$, q is the photon transverse momentum, σ is the width of the Gaussian transverse paths, and d is the spatial distance between the center of the paths. The states $\{|v\rangle_x\}$ form a basis in the three-dimensional state space [29] and the state in Eq. (1) represents a tensor product of a coherent superposition of the possible transverse path state components $|v\rangle_x$ and a fixed y mode and polarization. The polarization can be regarded as an auxiliary system while the main system initially prepared in the \hat{x} -direction paths will be transformed to paths that are qutrits in the \hat{y} direction. The first step of the transformation is to use a well-chosen \hat{y} -oriented diffraction grating centered at each $x = \nu$, implementing $|v\rangle_x \otimes |0\rangle_y \mapsto \sum_m c_{m\nu} |v\rangle_x \otimes |m\rangle_y$. A spatial filter is used to select the new Gaussian paths in the \hat{y} direction by filtering only the diffraction orders -1 , 0 , and 1 . After the spatial filter, the state becomes $|\Psi'\rangle \propto \sum_{m=-1}^1 \sum_{\nu=0}^2 c_{m\nu} A_{\nu} |v\rangle_x \otimes |m\rangle_y \otimes |H\rangle$, where $|m\rangle_y$ represents one Gaussian beam centered in $y = m$. The three initial paths can, in principle, generate nine Gaussian paths, as shown in Fig. 1. The superposition of the three paths with Gaussian transversal profiles along \hat{x} is necessary to obtain a qutrit path state in the \hat{y} direction. It can be achieved by using an interferometer based on calcite beam displacers, as shown in Fig. 1. After the spatial filtering, a half-wave plate (HWP) is positioned in the \hat{x} paths 1 and 2 in order to perform the polarization transformation $|H\rangle \mapsto |V\rangle$, where $|V\rangle$ stands for the vertical polarization state. In this way only path 0 suffers a spatial shift after the beam displacer, $|0\rangle_x \mapsto |1\rangle_x$. At this stage, the beams do not have the same polarization state. A HWP oriented at 22.5° with respect to the horizontal axis (x -direction) and a PBS is used to select the $|H\rangle$ polarization component, at the cost of half of the intensity. This same procedure is repeated to recombine the two remaining beams. After the second PBS we finally disentangle \hat{x} , \hat{y} , and the

polarization, and obtain the transformed state in \hat{y} space,

$$|\Psi\rangle_f \propto \sum_{m=-1}^1 (A_0 c_{m0} + A_1 c_{m1} + A_2 c_{m2}) |m\rangle_y. \quad (2)$$

Equation (2) shows that this setup is capable of implementing a large class of state transformations in an automated way, since the initial-state amplitudes are modified by the appropriate choice of diffraction gratings at the initial path ν . As pointed out above, the polarization degree of freedom is an auxiliary degree of freedom to perform transformations in the transverse path modes, since these transformations are independent of the number of photons in each path mode. The attenuated laser beam in the setup of Fig. 1 can be substituted by an intense laser beam, such that optical intensities can be detected instead of the detection of the single photon. An intense laser beam was used to demonstrate the ability of our setup to realize qutrit operations.

III. RESULTS AND DISCUSSIONS

We now report the implementations of projections onto specific subspaces, as well as some basic operations such as identity and permutations. Let us first consider the projection in the computational basis state $|1\rangle = (0, 1, 0)^T$, where the superscript T means transposition. This operation is very simple for the usual slit setup, so it is important to show that this general method can also achieve it. In our experimental setup, this means that the interferometer should discard any signal coming from paths $\nu = 0, 2$, while the path $\nu = 1$ should feed the output state $m = 0$. To achieve such requirements, we implement a blazed diffraction grating (BZDG) [29] in the 0 and 2 paths, which linearly increases (or decreases) the phase from 0 to 2π (2π to 0) inside a period. Such a periodic phase profile diffracts each of the beams at the 0 (2) path to the -1 ($+1$) diffraction order [29]. If we set the period to be short enough, these diffracted orders can be blocked by the spatial filter inserted in the interferometer. This procedure to block some photon paths is also automated, through the SLM, and will be present in almost all cases shown here. On the other hand, the path $\nu = 1$ needs only to be reflected by the SLM, i.e., with no diffraction. Projections on the remaining states of the computational basis, $|0\rangle = (1, 0, 0)^T$ and $|2\rangle = (0, 0, 1)^T$, follow ideas similar to the last one. For the first one, we use at path 0 a crescent BZDG with phase values 0 to 2π in a period T , so this path state component is diffracted in the order $+1$. This period must be large enough to avoid blocking by the spatial filter, while paths 1 and 2 are blocked as described above. The projection on the last state uses a decreasing BZDG at path 2, and components 0 and 1 are blocked.

Figures 2(a)–2(c) show the experimental results of the use of our quantum operation setup for projections at the computational basis. The optical beams are prepared in the initial state $|\psi_i\rangle = |1\rangle_x$ and the apparatus performs the projection in each of the three computational basis states. The CCD camera registers the transverse profile of the transmitted optical beams at the end of the interferometer (Fig. 1). We integrated the optical profile in the \hat{x} transverse direction and called it the *integrated transverse optical profile* (ITOP). We obtain a significant readout only in the case of projection in the same

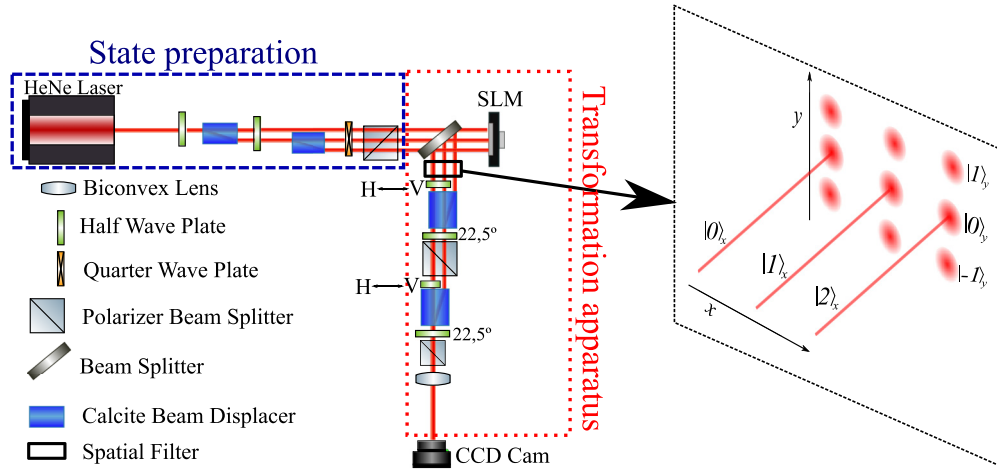


FIG. 1. Experimental setup. State preparation consists of wave plates, calcite \hat{x} -beam displacers, and a polarizer, in order to prepare $|\Psi\rangle$ shown in (1). The transformation apparatus consists in actuating in each path with a specific \hat{y} -diffraction grating, using the programmable phase-only reflection SLM (Hamamatsu, model LCOS-SLM X1046801), and a sequence of wave plates, calcite \hat{x} -beam displacers, PBS, and spatial filters in order to recombine the beam transformed as $|\Psi'\rangle$ shown in (2). In the right-hand panel, the effect of the spatial filter is highlighted, with each of the three \hat{x} paths generating three \hat{y} orders of diffraction. After a collimating lens, the final readout is accomplished by a CCD.

initial state [Fig. 2(a)], while in the case of orthogonal state projection we just observe a noise level signal [Figs. 2(b) and 2(c)], as expected. Notice that the final path state is well fitted by a Gaussian profile, as showed by the continuous red line in Fig. 2(a).

We can also perform projections at the superposition states $|\psi_f\rangle = (1,0,1)^T$ and $|\psi_f\rangle = (1,0,-1)^T$. In the first case, we use triangular phase grating profiles of height 2π and period T at paths 0 and 2 [29]. Such a grating consists of a crescent linear function at a spatial interval $[0, T/2]$ and a decreasing linear function at $[T/2, T]$. In this condition, $c_{1v} = c_{-1v}$, while $c_{0v} = 0$. Path 1 is blocked, as explained above. Figures 2(d) and 2(e) show the final ITOP when the initial states are $|\psi_i\rangle = |0\rangle_x$ and $|\psi_i\rangle \propto |0\rangle_x + |1\rangle_x$, respectively. In order to implement projection at the state $|\psi_f\rangle = (1,0,-1)^T$, we could perform the same operation proposed for $|\psi_f\rangle = (1,0,1)^T$, except we now need to add a π phase at some diffraction orders. In this case, the use of an extra transmission phase-only SLM would be a good option, but an alternative way was chosen. At paths 0 and 2 we use a binary phase grating (BPG) of height π and period T [29]. Figures 2(f) and 2(g) show the results obtained by using this strategy for two different nonorthogonal initial states (again $|\psi_i\rangle = |0\rangle_x$ and $|\psi_i\rangle \propto |0\rangle_x + |1\rangle_x$). Gaussian fits of the transverse light intensity reveal that the final path state components remain with a good Gaussian profile after projection.

A state projection that is worth discussing is the projection over $|\psi_f\rangle = (-1,1,1)^T$. In this case, we set a binary phase grating (BPG) of height $2\arctan(\pi/2)$ in all paths, which should distribute the initial-state components equally among the components of the final state [29] and with the correct relative phases. The only difference between the three BPGs in each path is that the grating at path 0 has an additional phase of π in all diffraction orders. In Fig. 2(h), we show the ITOP for the projection of the initial state $|\psi_i\rangle = |0\rangle_x$.

By projecting onto one of the basis states, we just generate a Gaussian packet. However, the other states generated by the

already discussed projections are much richer, in the sense that the spatial interference between path modes gives extra information about the projected state.

Important information given by the interference pattern is the relative phases between the path components. This information can be obtained by fitting the resulting pattern using a generic equation for the three-path interference given by

$$I(q) = Ne^{-(\sigma kx/f)} \{ |a|^2 + |b|^2 + |c|^2 + 2[|a||b| \cos(2\pi qd + \phi_{ab}) + |b||c| \cos(2\pi qd + \phi_{ab} + \phi_{ac}) + |a||c| \cos(4\pi qd + \phi_{ac})] \}, \quad (3)$$

where a , b , and c , are the complex amplitudes of a general three-path initial state, d is the Gaussian path separations, σ is the Gaussian path width, $\phi_{b(c)}$ are the phase differences between the paths with amplitudes b (c) in relation to path a , and the transverse momentum is given by $q = kx/f$, in the case where a spherical lens is used to project the Fourier plane at the detector plane. The relative phases in this case are the free parameters of the fit, while the other parameters are extracted from the experimental transverse path profile at the image plane.

In order to test it, we use another spherical lens ($f = 30$ cm) and detect the interference pattern with the CCD at the Fourier plane. Figure 3(a) shows the spatial interference patterns with the projected Gaussian states $|\psi_f\rangle = (1,0,-1)^T$ (blue square) and $|\psi_f\rangle = (1,0,1)^T$ (red dot). One can see the phase shift between the two Gaussian interference patterns, suggesting the orthogonality of the two subspaces explored. Figure 3(b) shows the interference pattern between the spatial modes of the projected state $|\psi_f\rangle = (-1,1,1)^T$. The small peaks in Fig. 3(b) are characteristic of three Gaussian interference patterns and the high visibility indicates that the state coherence is preserved after the operation.

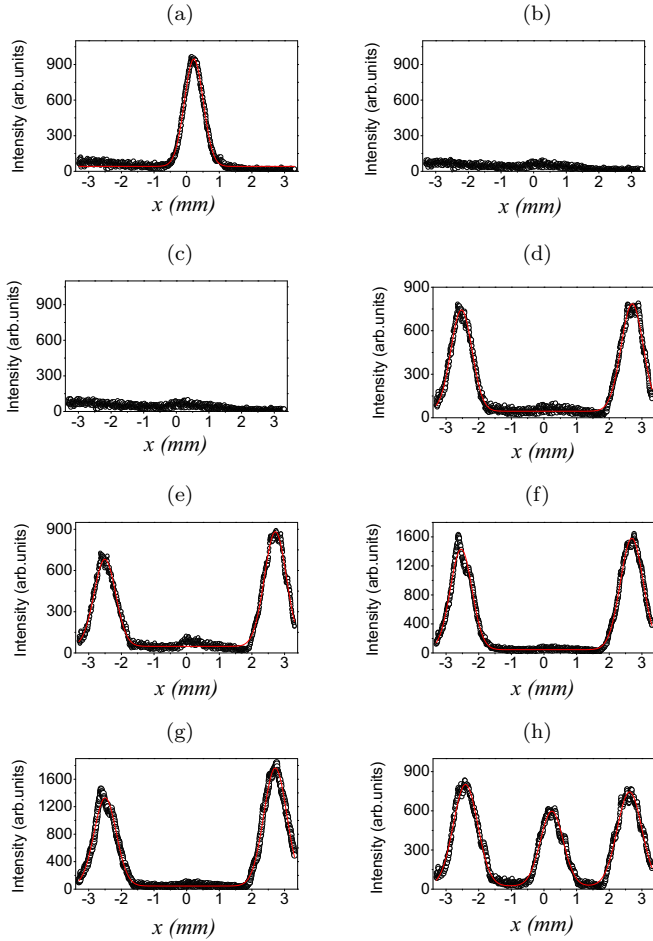


FIG. 2. Integrated transverse optical profile (ITOP) of resulting states after performing the operations. (a)–(c) Projections onto computational basis states $(0, 1, 0)^T$, $(0, 0, 1)^T$, and $(0, 0, 1)^T$, respectively. The initial state is fixed as $|\psi_i\rangle = |1\rangle_x$. The continuous red line represents a Gaussian fit. In (d) and (e), the black circles register the projection onto $(1, 0, 1)^T$ for the initial states (d) $|\psi_i\rangle = |0\rangle_x$ and (e) $|\psi_i\rangle \propto |0\rangle_x + |1\rangle_x$, while the continuous red line represents a two-Gaussian fit. In (f) and (g), projection onto $(1, 0, -1)^T$ for the initial states (f) $|\psi_i\rangle = |0\rangle_x$ and (g) $|\psi_i\rangle \propto |0\rangle_x + |1\rangle_x$, while the continuous red line represents a two-Gaussian fit. In (h), projection onto $(-1, 1, 1)^T$ for the initial state $|\psi_i\rangle = |0\rangle_x$, with a three-Gaussian fit (continuous red line).

Using the relative path phases obtained from the interference pattern and the path amplitudes of the projected states [obtained by integrating and normalizing the Gaussian area of Figs. 2(d)–2(h)], we can characterize the projected state and calculate the fidelity with the ideal projected states. For the projected states $|\psi_f\rangle = (1, 0, 1)^T$ and $|\psi_f\rangle = (1, 0, -1)^T$, the calculated fidelities to the respective ideal states are $f = 0.92 \pm 0.04$ and $f = 0.98 \pm 0.04$, respectively, while the fidelity for the projected state $|\psi_f\rangle = (-1, 1, 1)^T$ is $f = 0.73 \pm 0.06$.

Since this method encodes input and output states in different spaces, \hat{x} and \hat{y} path states, the identity operator cannot be implemented as doing nothing. As discussed above, we define identity as the operator $|\nu\rangle_x \mapsto |\nu - 1\rangle_y$, but now we need to program the SLM to implement this

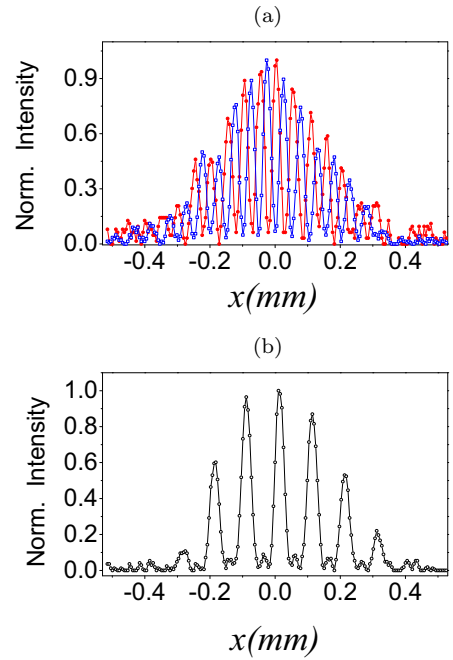


FIG. 3. Interference patterns at the Fourier plane. (a) Interference fringes after projection onto $(1, 0, -1)^T$ (blue square) and $(1, 0, 1)^T$ (red dot). (b) Interference fringes after projection onto $(-1, 1, 1)^T$. In all cases, the solid lines just link the points.

transformation. The approach we took was to use a negative slope BZDG of height 2π at path 0, no phase grating at path 1, and a positive slope BZDG of height 2π at path 2. Another class of operations implemented by using the BZDG is the permutation operations. They just interchange coefficients of the state components. While the identity was defined by $\{|0\rangle_x, |1\rangle_x, |2\rangle_x\} \mapsto \{|-1\rangle_y, |0\rangle_y, |1\rangle_y\}$, a cyclic right permutation, for instance, is given by $\{|0\rangle_x, |1\rangle_x, |2\rangle_x\} \mapsto \{|0\rangle_y, |1\rangle_y, |-1\rangle_y\}$. Experimentally, the only difference is in which paths ν the positive and negative slope BZDG gratings will act on. Such permutation operations can be used as logical gates and are clearly nondiagonal. Any other permutation can be similarly implemented. Figure 4 shows the ITOP after the identity operation (blue squares) and the cyclic right permutation operation (black circles) are applied to

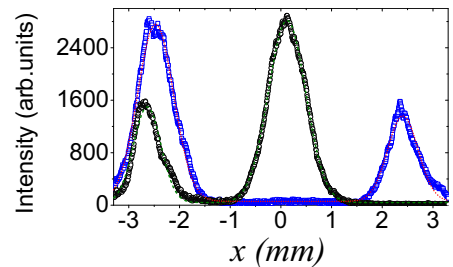


FIG. 4. Integrated transverse optical profiles (ITOPs) for identity and cyclic right permutation applied to the state $|\psi_i\rangle = A_0|0\rangle_x + A_2|2\rangle_x$, in which $|A_0| > |A_2|$. Blue squares stand for the data from the identity operation, with the red dotted line a two-Gaussian fit, while black circles show the permutation operation, with the green dashed line the corresponding two-Gaussian fit.

an initial state $|\psi_i\rangle = A_0|0\rangle_x + A_2|2\rangle_x$, in which $|A_0| > |A_2|$. The quality of the permutation operation can be estimated by performing the inner product of the ideal permuted state ($|\psi_{\text{ideal}}\rangle$) with the experimentally permuted state ($|\psi'\rangle$). We will assume that the ideal permuted state is the measured qutrit state after the identity operation with the coefficients is permuted. Since there are no phases added to the diffraction order for the BZDG grating used, the states $|\psi_{\text{ideal}}\rangle$ and $|\psi'\rangle$ can be obtained from the experimental data by calculating the path amplitudes of the experimental states after the identity and permutation operations. These states are given by

$$\begin{aligned} |\psi_{\text{ideal}}\rangle &= \sqrt{0.31}|0\rangle + \sqrt{0.69}|1\rangle, \\ |\psi'\rangle &= \sqrt{0.29}|0\rangle + \sqrt{0.71}|1\rangle. \end{aligned} \quad (4)$$

The inner product $\langle\psi_{\text{ideal}}||\psi'\rangle = 0.99 \pm 0.04$, revealing that the state after the permutation operation can be regarded as the state after the identity operation with their amplitudes interchanged.

We may not be able to implement an arbitrary three-dimensional projector, but we can implement a great number of them, modifying the type of phase grating, its height, and its period. On the other hand, a tomographically complete set of projectors can be implemented. We are able to perform state tomography in spatial qutrits by using, for example, the symmetric informationally complete positive operator-valued measure (SIC-POVM) discussed in Refs. [31,32]. For one qutrit state there are nine POVM elements, $\hat{M} \propto |\psi_k\rangle\langle\psi_k|$, with $k = 1, 2, \dots, 9$, and $|\psi_k\rangle$ are given by

$$\begin{aligned} |\psi_1\rangle &\propto |0\rangle + |2\rangle, \\ |\psi_2\rangle &\propto e^{i\phi}|0\rangle + e^{-i\phi}|2\rangle, \\ |\psi_3\rangle &\propto e^{-i\phi}|0\rangle + e^{i\phi}|2\rangle, \\ |\psi_4\rangle &\propto |1\rangle + |0\rangle, \\ |\psi_5\rangle &\propto e^{i\phi}|1\rangle + e^{-i\phi}|0\rangle, \\ |\psi_6\rangle &\propto e^{i\phi}|1\rangle + e^{-i\phi}|0\rangle, \\ |\psi_7\rangle &\propto |2\rangle + |1\rangle, \\ |\psi_8\rangle &\propto e^{i\phi}|2\rangle + e^{-i\phi}|1\rangle, \\ |\psi_9\rangle &\propto e^{-i\phi}|2\rangle + e^{i\phi}|1\rangle, \end{aligned} \quad (5)$$

where $\phi = 2\pi/3$. These can be implemented by a similar strategy used for the $(1, 0, 1)^T$ projectors plus a constant phase in one of the two paths.

Two aspects are important when single photons from a heralded spontaneous parametric down-conversion (SPDC) source are used in the setup: coherence and efficiency in implementing the operations. Interference is essential in the state transformation part of the setup, requiring that the length differences between the interferometer arms be smaller than the single-photon coherence length. This can be achieved with birefringent materials for temporal delay compensation, as shown in Ref. [29]. Temporal delay compensation is not necessary though if narrow-band frequency photon pairs produced by cavity-enhanced SPDC are used [33].

This means that the setup used here can be adapted with few changes to work with SPDC photon sources. Figure 5 shows an example of a setup that can be used with single

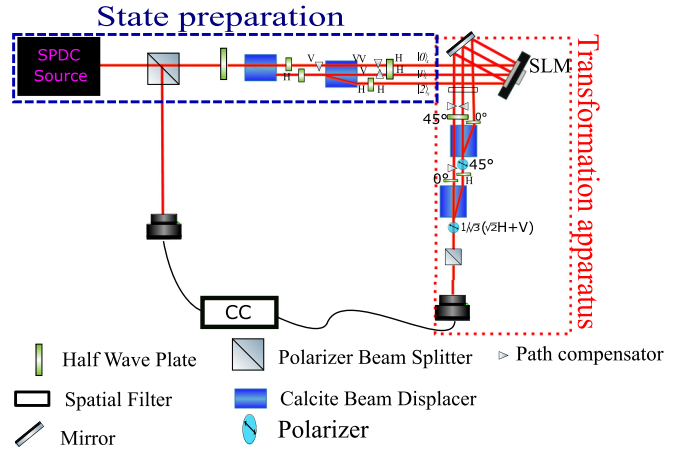


FIG. 5. Experimental setup to prepare and operate over a qutrit state encoded at the transverse paths of a single-photon heralded source (spontaneous parametric down-conversion).

photons from a heralded SPDC regular source. All beams pass inside the calcites and D-shaped wave plates are used such that the path differences can be compensated and the polarizations of the modes are independently rotated, as shown in Ref. [34]. Concerning the second aspect (efficiency), the setup presented here has losses that can be overcome in future realizations with single-photon sources. For instance, losses in the state preparation can be reduced to a few percent with some suitable changes. The SLM can be set for oblique reflection, avoiding the losses due to the beam splitter; D-shaped half-wave plates can be used for rotating the polarization of each mode individually [34], temporal delay compensation can be used, and the first PBS removed. The angles in which the polarization projections are made can be optimized to minimize losses [29]. However, all losses due to spatial filtering or polarization projection strongly depend on the operation to be implemented. For the cases studied here, the projection in the state $(1, 1, -1)^T$ can achieve 86% probability of actually having the operation implemented, while the projection in the state $(1, 0, 1)^T$ reaches only 24% probability of success. This difference is due to the efficiency of the grating, revealing the strong dependency of the losses with respect to the specific grating used to achieve each operation. If only permutation operations are performed, path information need not be erased at all and only a sawtooth grating is necessary. The relevant parameter in this operation is the SLM diffraction efficiency, in our case near 94%.

IV. CONCLUSIONS

We demonstrate the possibility of the automated state manipulation of spatial photonics in qutrits in the laboratory. The experimental approach explored in this work already confirms the possibility of an operation on qutrits encoded in transverse photon paths in an automated way, surpassing a barrier for its use in the implementation of quantum computation and quantum fundamental tests. This opens a wide range of applications, such as simulating quantum open system dynamics, manipulation of twin photon states, and fundamental tests, such as sequential measurements in noncontextuality tests.

ACKNOWLEDGMENTS

We are grateful for support from the Brazilian agencies CNPq, CAPES, FAPESP, and FAPEMIG. B.M. and R.B. are

supported by FAPESP No. 2014/27223-2 and FAPESP No. 2016/24162-8, respectively. We are thankful to R. Rabelo for useful discussions.

-
- [1] S. Kochen and E. P. Specker, *J. Math. Mech.* **17**, 59 (1967).
- [2] B. Marques, J. Ahrens, M. Nawareg, A. Cabello, and M. Bourennane, *Phys. Rev. Lett.* **113**, 250403 (2014).
- [3] X.-M. Hu, J.-S. Chen, B.-H. Liu, Y. Guo, Y.-F. Huang, Z.-Q. Zhou, Y.-J. Han, C.-F. Li, and G.-C. Guo, *Phys. Rev. Lett.* **117**, 170403 (2016).
- [4] M. Genovese and P. Traina, *Adv. Sci. Lett.* **1**, 153 (2008).
- [5] A. C. Dada, J. Leach, G. S. Buller, M. J. Padgett, and E. Andersson, *Nat. Phys.* **7**, 677 (2011).
- [6] D. P. O’Leary, G. K. Brennen, and S. S. Bullock, *Phys. Rev. A* **74**, 032334 (2006).
- [7] N. K. Langford, R. B. Dalton, M. D. Harvey, J. L. O’Brien, G. J. Pryde, A. Gilchrist, S. D. Bartlett, and A. G. White, *Phys. Rev. Lett.* **93**, 053601 (2004).
- [8] S. Etcheverry, G. Cañas, E. Gómez, W. Nogueira, C. Saavedra, G. Xavier, and G. Lima, *Sci. Rep.* **3**, 2316 (2013).
- [9] S. P. Walborn, D. S. Lemelle, M. P. Almeida, and P. H. Souto Ribeiro, *Phys. Rev. Lett.* **96**, 090501 (2006).
- [10] W. M. Pimenta, B. Marques, M. A. D. Carvalho, M. R. Barros, J. G. Fonseca, J. Ferraz, M. T. Cunha, and S. Pádua, *Opt. Express* **18**, 24423 (2010).
- [11] G. Taguchi, T. Dougakiuchi, N. Yoshimoto, K. Kasai, M. Iinuma, H. F. Hofmann, and Y. Kadoya, *Phys. Rev. A* **78**, 012307 (2008).
- [12] G. Lima, L. Neves, R. Guzmán, E. S. Gómez, W. A. T. Nogueira, A. Delgado, A. Vargas, and C. Saavedra, *Opt. Express* **19**, 3542 (2011).
- [13] M. Agnew, J. Leach, M. McLaren, F. S. Roux, and R. W. Boyd, *Phys. Rev. A* **84**, 062101 (2011).
- [14] E. V. Kovlakov, I. B. Bobrov, S. S. Straupe, and S. P. Kulik, *Phys. Rev. Lett.* **118**, 030503 (2017).
- [15] H. Di Lorenzo Pires, H. C. B. Florijn, and M. P. van Exter, *Phys. Rev. Lett.* **104**, 020505 (2010).
- [16] A. J. Gutiérrez-Esparza, W. M. Pimenta, B. Marques, A. A. Matoso, J. L. Lucio M., and S. Pádua, *Opt. Express* **20**, 26351 (2012).
- [17] M. Agnew, J. Leach, and R. Boyd, *Eur. Phys. J. D* **66**, 156 (2012).
- [18] A. Vaziri, J.-W. Pan, T. Jennewein, G. Weihs, and A. Zeilinger, *Phys. Rev. Lett.* **91**, 227902 (2003).
- [19] B. Marques, A. A. Matoso, W. M. Pimenta, A. J. Gutiérrez-Esparza, M. F. Santos, and S. Pádua, *Sci. Rep.* **5**, 16049 (2015).
- [20] E. Nagali, L. Sansoni, F. Sciarrino, F. De Martini, L. Marrucci, B. Piccirillo, E. Karimi, and E. Santamato, *Nat. Photonics* **3**, 720 (2009).
- [21] G. Borges, M. Carvalho, P.-L. de Assis, J. Ferraz, M. Araújo, A. Cabello, M. T. Cunha, and S. Pádua, *Phys. Rev. A* **89**, 052106 (2014).
- [22] G. Cañas, S. Etcheverry, E. S. Gómez, C. Saavedra, G. B. Xavier, G. Lima, and A. Cabello, *Phys. Rev. A* **90**, 012119 (2014).
- [23] L. Neves, G. Lima, J. G. Aguirre Gómez, C. H. Monken, C. Saavedra, and S. Pádua, *Phys. Rev. Lett.* **94**, 100501 (2005).
- [24] M. A. Solís-Prosser, A. Arias, J. J. M. Varga, L. Rebón, S. Ledesma, C. Iemmi, and L. Neves, *Opt. Lett.* **38**, 4762 (2013).
- [25] G. Cañas, M. Arias, S. Etcheverry, E. S. Gómez, A. Cabello, G. B. Xavier, and G. Lima, *Phys. Rev. Lett.* **113**, 090404 (2014).
- [26] G. Lima, L. Neves, I. F. Santos, J. G. Aguirre Gómez, C. Saavedra, and S. Pádua, *Phys. Rev. A* **73**, 032340 (2006).
- [27] A. J. Gutiérrez-Esparza, W. M. Pimenta, B. Marques, A. A. Matoso, J. Sperling, W. Vogel, and S. Pádua, *Phys. Rev. A* **90**, 032328 (2014).
- [28] A. F. Abouraddy, G. Di Giuseppe, T. M. Yarnall, M. C. Teich, and B. E. A. Saleh, *Phys. Rev. A* **86**, 050303 (2012).
- [29] R. D. Baldijão, G. F. Borges, B. Marques, M. A. Solís-Prosser, L. Neves, and S. Pádua, *Phys. Rev. A* **96**, 032329 (2017).
- [30] C. Zu, Y.-X. Wang, D.-L. Deng, X.-Y. Chang, K. Liu, P.-Y. Hou, H.-X. Yang, and L.-M. Duan, *Phys. Rev. Lett.* **109**, 150401 (2012).
- [31] C. Paiva-Sánchez, E. Burgos-Inostroza, O. Jiménez, and A. Delgado, *Phys. Rev. A* **82**, 032115 (2010).
- [32] W. M. Pimenta, B. Marques, T. O. Maciel, R. O. Vianna, A. Delgado, C. Saavedra, and S. Pádua, *Phys. Rev. A* **88**, 012112 (2013).
- [33] K.-H. Luo, H. Herrmann, S. Krapick, B. Brecht, R. Ricken, V. Quiring, H. Suche, W. Sohler, and C. Silberhorn, *New J. Phys.* **17**, 073039 (2015).
- [34] G. H. Aguilar, A. Valdés-Hernández, L. Davidovich, S. P. Walborn, and P. H. Souto Ribeiro, *Phys. Rev. Lett.* **113**, 240501 (2014).